ORIGINAL PAPER

ZAMM

Comprehensive elastic analysis of functionally graded variable thickness pressurized disk

Ömer Can Farukoğlu[1,2] | **Ihsan Korkut[1]** | **Ali Motameni[2,3]**

[1]Department of Manufacturing Engineering, Gazi University, Ankara, Turkey

[2]Department of Mechanical Engineering, Çankaya University, Ankara, Turkey

[3]Department of Metallurgical and Materials Engineering, Middle East Technical University, Ankara, Turkey

Correspondence
Ömer Can, Farukoğlu, Department of Manufacturing Engineering, Gazi University, Emniyet Dist., 06560 Yenimahalle, Ankara, Turkey.
Email: omercan.farukoglu@gazi.edu.tr

This study analytically examines internally pressurized power-law functionally graded variable thickness disk. The power-law consideration is applied to the Young's modulus and the Poisson's ratio of the graded material as well as the radial thickness profile variation of the disk. Under this scheme, the solution yields to different Bessel functions including the first, second, and modified types. Stress and displacement fields are investigated at the elastic limits by operating with these functions. The limits are calculated with the well-known von Mises criteria. Following the analytical modeling, numerical examples are built. Therein the examples, some noteworthy nuances have been achieved. It has been observed that unlike the usual prediction in the literature, constant Poisson's ratio, the effect of variable Poisson's ratio on stresses and displacements is still evident, although not as much as variable Young's modulus and disk geometry. We suggest assigning it as a variable in similar applications to be more precise. Additionally, according to the von Mises criterion, yielding may begin at the inner radius, the outer radius, or both at the same time. Parameters in the simultaneous flow initiation state are critical. These parameters allow the disk to reach the highest elastic limit pressure.

1 | INTRODUCTION

Functionally graded materials can be described as a material type where the mechanical properties gradually alter at the desired direction in accordance with the engineering application. The grading concept began in the early 1970s for polymeric materials, but the first application was in 1984 in the space shuttle project of Japan, wherein a thermal shielding that is, able to withstand a 1000°C-temperature difference at a 10 mm wall thickness was needed. The purpose was to manufacture a material that can overcome this temperature gradient [1, 2]. Over the years, this material concept became popular and since then it has been actively employed in various engineering sectors such as automotive, nuclear or biomedical. Even though functionally graded materials were designed for thermal resistance in the initiation phase, later it was used to control stress fields in the pressurized elements as well. Various studies have been performed in this regard for pressurized disks, cylinders, or spheres, yet there are still various questions to seek answers to. Herein, some of the interesting and influential stress investigations on graded cylindrical or spherical components are compiled. In this context, internally and/or externally pressurized annular disks made of functionally graded materials and their elastic state stresses have been studied with closed-form [3–5] and finite element solutions [6]. Pressurized cylinders and tubes at the elastic-plastic state are topics of previous examinations [7–9]. In a recent study, both exact and finite element solutions on the functionally graded disk have been compared [10]. In the scientific literature, there are studies that consider graded cylinders subjected to not only pressure loads but also thermal [8, 11] or magnetic fields [12]. Investigations concerning functionally

graded pressure vessels under different loading conditions are also present, which are cylindrical [13–15] and spherical [16–20]. Regarding the references mentioned in the previous sentence, it is to be mentioned that some studies only took mechanical loads into account [13, 15, 16]. On the other hand, some investigations have considered both thermal and mechanical loading conditions in pressure vessels [14, 17–20]. Since cylindrical and spherical components resemble, some researchers have proposed a mathematical technique, which is called complementary functions method, for uniformly pressurized functionally graded components [21]. In some industrial applications, instead of manufacturing the whole pressurized axisymmetric component with the graded material, combining homogeneous material with graded coating is another engineering design method. In this respect, the following two researches can be looked into [22, 23].

In mathematical solution procedures, there are some studies that implement power series technique as well. For instance, the authors proposed an elastic solution for pressurized graded cylindrical and spherical pressure vessels where the Young's modulus is modeled with $E(r) = E_o \exp[\beta(r - a)/(b - a)]$ [24]. The power series solution with the stress function approach is implemented thereat. By the same token, the researcher propounded a stress analysis with the method of Frobenius for pressurized thick-walled graded cylinders wherein the Young's modulus is an exponential function as $E(r) = E_o \exp[\beta r]$ [25]. The thermo-mechanically loaded short cylinder of graded material has been handled at another related research, where the stresses in the geometry are modeled via using the Fourier series [26]. While the Young's modulus and thermal expansion coefficients are considered as power-law functions, Poisson's ratio was taken as constant. In a similar vein, applying the Legendre series to poro-piezo hollow spheres of graded material, thermo-mechanical stresses are investigated [27].

Except for an additional body force term to the equilibrium equation and change of the applied boundary conditions, rotating axisymmetric graded components share a parallel solution procedure with pressurized ones. Hence, some of these studies can be mentioned as well. Correspondingly, various studies can be checked for stresses of rotating functionally graded hollow shafts [28–30] and cylinders [31]. In addition, rotating graded disks have been extensively examined. Functionally graded rotating annular hollow disks at the elastic region have been a topic of some investigations [32, 33]. When the disk thickness variation is considered, there exists plenty of examinations [34–39]. Moreover, there are some extended stress studies for variable profile rotating graded disks at elastic-plastic state under thermo-mechanical loads [40, 41].

Following the exhibition of related investigations in the existing literature, we may return to the purpose of this research. In this study, at the elastic limits, stress and displacement states of the internally pressurized disk are going to be discussed thoroughly. Additionally, unlike the common assumption in related researches, which is the constant Poisson's ratio consideration, we have taken it as a variable. In examinations that consider power-law as a grading rule [3, 5, 14–15, 17, 19, 23, 26–30, 42], none of them have taken Poisson's ratio as a variable. Moreover, at the current state of the literature most disk investigations often focus on the elastic state stresses not the elastic limits. By paying attention to the limits, this paper may broaden the current state. It should be noted that there are investigations that considers above elastic state stress fields. However, in these fields generally the interest is given to elastic-plastic or fully plastic zones not the elastic limits. Due to these reasons, this work might be considered as an alternative to the research area. Herein, the grading and disk thickness vary along radius r by the power-law. Young's modulus ($E(r)$), Poisson's ratio ($v(r)$), and disk profile ($h(r)$) are modeled accordingly. These properties are

$$E(r) = E_o \left[\frac{r}{b}\right]^\alpha, \tag{1}$$

$$v(r) = v_o \left[\frac{r}{b}\right]^\beta, \tag{2}$$

$$h(r) = h_b \left[\frac{r}{b}\right]^g, \tag{3}$$

in which E_o and v_o are the reference values of the corresponding properties and α, β are the grading parameters. In Equation (3), h_b is the thickness of the disk at $r = b$ and g is the geometric parameter. The disk is demonstrated pictorially in Figure 1. While developing this research, one comment we received was grading parameters (α, β) of Young's modulus and Poisson's ratio should be related. In a way, this comment is both agreeable and disagreeable. It is true that grading parameters should be connected. However, the direct relationship between grading parameters is not clear. In some articles such as [19], grading parameters of various material properties have been taken as equal. So, one parameter homogenization
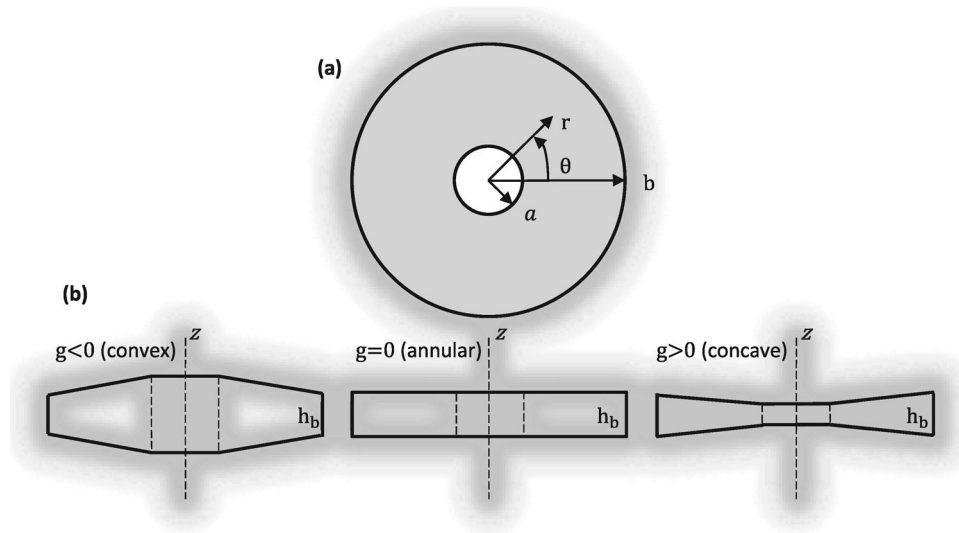
FIGURE 1 Disk's (a) top view and (b) side profile illustrations.

has been considered thereat. On the other hand, in another related papers [5, 42], different values have been assigned to grading parameters. Therefore, it is appropriate to state that grading parameters should be related, yet, the degree of this relation is not clear. It could be equal, proportional, or not related at all. In the numerical examples of this paper, we have kept one grading parameter constant and varied the other to observe the effect of the particular grading parameter. Another important point is the disk thickness profile. Herein, in order to be in harmony with the properties, power-law is applied to the disk profile. The profile can be any reasonable function since material grading and disk profile are two separate quantities. Depending on the design parameters of the project, disk profile should be considered accordingly. In the literature, assigning both properties and disk thickness profile to similar functions is a common practice, for instance reference [36]. Additionally, it should be pointed out that profile variation function highly changes the solution procedure to be followed. Different profiles may yield to analytical, semi-analytical or fully numerical approaches.

2 | ANALYTICAL SOLUTION

In the fundamental elastic relations, infinitesimal deformations and the state of plane stress are considered. While exhibiting such relations, the cylindrical polar coordinate system is used. Elastic strain-displacements relations can be designated as

$$\epsilon_r = \frac{du}{dr} , \epsilon_\theta = \frac{u}{r}, \tag{4}$$

in which $\epsilon_r = \epsilon_r(r)$ and $\epsilon_\theta = \epsilon_\theta(r)$ express elastic strains in r and θ directions. Also, u = u(r) denotes radial displacement. From the generalized Hooke's law, strain-stress relations are introduced below

$$\epsilon_r = \frac{du}{dr} = \frac{1}{E(r)}\left[\sigma_r - v(r)\sigma_\theta\right], \tag{5}$$

$$\epsilon_\theta = \frac{u}{r} = \frac{1}{E(r)}\left[\sigma_\theta - v(r)\sigma_r\right], \tag{6}$$

where $\sigma_r = \sigma_r(r)$ and $\sigma_\theta = \sigma_\theta(r)$ terms are the stress components in the related directions. For the mechanical analysis herein, equilibrium equation is

$$\frac{d}{dr}\left[h(r)r\sigma_r\right] - h(r)\sigma_\theta = 0, \tag{7}$$

and the compatibility condition is of the form

$$\frac{d}{dr}[r\in_\theta] - \in_r = 0. \tag{8}$$

Using the equilibrium equation, tangential stress can be written as

$$\sigma_\theta = \sigma_r + r\frac{d\sigma_r}{dr} + r\frac{\sigma_r}{h(r)}\frac{dh(r)}{dr}. \tag{9}$$

Inserting Equation (9) into (6) and multiplying the equation by r, the radial displacement is obtained

$$u = \frac{r}{E(r)}\left[\{1 - v(r)\}\sigma_r + r\frac{d\sigma_r}{dr} + r\frac{\sigma_r}{h(r)}\frac{dh(r)}{dr}\right]. \tag{10}$$

As can be seen from Equations (9) and (10), we have connected tangential stress and radial displacement to the radial stress and its derivative. This means that when the radial stress is found, one is able to achieve tangential stress and radial displacement as well. In this context, let's plug in Equations (1)–(3), and (9) into directional strains in Equations (5) and (6). After this operation, the corresponding $\in_r$ and $\in_\theta$ are substituted into the compatibility condition, which yields to

$$r^2\frac{d^2\sigma_r}{dr^2} + k_1 r\frac{d\sigma_r}{dr} + \left[k_2 r^\beta + k_3\right]\sigma_r = 0. \tag{11}$$

The following terms are determined to exhibit the above equation in a compact form

$$k_1 = 3 + g - \alpha, k_2 = v_o\ b^{-\beta}(g + \alpha - \beta), k_3 = g(1 - \alpha) - \alpha. \tag{12}$$

The governing equation (11) is a Bessel type differential equation and has various solutions depending on its parameters. Each possible solution is given separately:

Case 1: $k_2 > 0$ and n is a non-integer number

In this case, the radial stress emerges as

$$\sigma_r = r^{(1-k_1)/2}\left[C_1 J_n\left(\Omega r^{\beta/2}\right) + C_2 J_{-n}\left(\Omega r^{\beta/2}\right)\right]. \tag{13}$$

Herein, $J_n(\Omega r^{\beta/2})$ and $J_{-n}(\Omega r^{\beta/2})$ are the Bessel functions of the first kind, n is the order, and Ω is the argument of the functions. Additionally, C_1 and C_2 are the arbitrary constants. The function can be presented in series form

$$J_n\left(\Omega r^{\beta/2}\right) = \sum_{m=0}^\infty \frac{(-1)^m}{m!\Gamma(m + n + 1)}\left[\frac{\Omega r^{\beta/2}}{2}\right]^{2m+n}, \tag{14}$$

where Γ is the gamma function. If the n term in the above equation is replaced by -n, $J_{-n}(\Omega r^{\beta/2})$ can simply be found. The order and the argument are calculated with

$$n = \frac{\sqrt{(k_1 - 1)^2 - 4k_3}}{\beta}, \ \Omega = \frac{2\sqrt{k_2}}{\beta}. \tag{15}$$

Using Equations (3) and (13) with (9), tangential stress is obtained as

$$\sigma_\theta = \frac{r^{(1-k_1)/2}}{2}\left[C_1\left\{r^{\beta/2}\beta\Omega J_{n-1}\left(\Omega r^{\beta/2}\right) + (k_4 - n\beta)J_n\left(\Omega r^{\beta/2}\right)\right\} + C_2\left\{r^{\beta/2}\beta\Omega J_{-n-1}\left(\Omega r^{\beta/2}\right) + (k_4 + n\beta)J_{-n}\left(\Omega r^{\beta/2}\right)\right\}\right]. \tag{16}$$

Similar to the previous k_j terms, k_4 is determined

$$k_4 = 3 + 2g - k_1. \tag{17}$$

Combining Equations (1)–(3), (10) and (13), radial displacement is acquired

$$u = \frac{r^{(3-k_1)/2}}{2E_o} \left[\frac{r}{b}\right]^{-\alpha} \left[C_1 \left\{ r^{\beta/2}\beta\Omega\, J_{n-1}\left(\Omega r^{\beta/2}\right) + \left(k_4 - n\beta - 2v_o\left[\frac{r}{b}\right]^{\beta}\right) J_n\left(\Omega r^{\beta/2}\right)\right\} \right.$$
$$\left. + C_2 \left\{ r^{\beta/2}\beta\Omega\, J_{-n-1}\left(\Omega r^{\beta/2}\right) + \left(k_4 + n\beta - 2v_o\left[\frac{r}{b}\right]^{\beta}\right) J_{-n}\left(\Omega r^{\beta/2}\right)\right\}\right]. \tag{18}$$

In this study, the disk is subjected to internal pressure only. Thus, $\sigma_r(a) = -P$, $\sigma_r(b) = 0$ boundary conditions are applied to find C_1 and C_2. Here, a, b and P denote disk's inner radius, outer radius and the implemented pressure. Employing these conditions to Equation (13), we get C_1 and C_2 as

$$C_1 = -\frac{Pa^{(k_1-1)/2}J_{-n}\left(\Omega b^{\beta/2}\right)}{J_{-n}\left(\Omega b^{\beta/2}\right) J_n\left(\Omega a^{\beta/2}\right) - J_{-n}\left(\Omega a^{\beta/2}\right) J_n\left(\Omega b^{\beta/2}\right)}, \tag{19a}$$

$$C_2 = \frac{Pa^{(k_1-1)/2}J_n\left(\Omega b^{\beta/2}\right)}{J_{-n}\left(\Omega b^{\beta/2}\right) J_n\left(\Omega a^{\beta/2}\right) - J_{-n}\left(\Omega a^{\beta/2}\right) J_n\left(\Omega b^{\beta/2}\right)}. \tag{19b}$$

When $k_2 > 0$ and n is a non-integer number, the above stated solution occurs. In this case, $J_n(\Omega r^{\beta/2})$ and $J_{-n}(\Omega r^{\beta/2})$ are the linearly independent solutions of the governing differential equations. However, these functions are no longer independent if integer n is the case.

Case 2: $k_2 > 0$ and n is an integer number

When n is an integer value, the second solution of the radial stress changes from $J_{-n}(\Omega r^{\beta/2})$ to $Y_n(\Omega r^{\beta/2})$. The term $Y_n(\Omega r^{\beta/2})$ is the Bessel function of the second kind. Once again, the order and the argument are obtained with Equation (15). So, the radial stress is

$$\sigma_r = r^{(1-k_1)/2} \left[C_1 J_n\left(\Omega r^{\beta/2}\right) + C_2 Y_n\left(\Omega r^{\beta/2}\right)\right]. \tag{20}$$

The $Y_n(\Omega r^{\beta/2})$ is given by

$$Y_n\left(\Omega r^{\beta/2}\right) = \frac{J_n\left(\Omega r^{\beta/2}\right)\cos(n\pi) - J_{-n}\left(\Omega r^{\beta/2}\right)}{\sin(n\pi)}. \tag{21}$$

Utilizing Equations (3), (9) and (20), tangential stress yields to

$$\sigma_\theta = \frac{r^{(1-k_1)/2}}{2} \left[C_1 \left\{ r^{\beta/2}\beta\Omega J_{n-1}\left(\Omega r^{\beta/2}\right) + (k_4 - n\beta) J_n\left(\Omega r^{\beta/2}\right)\right\} + C_2 \left\{ r^{\beta/2}\beta\Omega Y_{n-1}\left(\Omega r^{\beta/2}\right) + (k_4 - n\beta) Y_n\left(\Omega r^{\beta/2}\right)\right\}\right]. \tag{22}$$

By using Equations (1)–(3), (10) and (20), radial displacement term is achieved

$$u = \frac{r^{(3-k_1)/2}}{2E_o} \left[\frac{r}{b}\right]^{-\alpha} \left[C_1 \left\{ r^{\beta/2}\beta\Omega\, J_{n-1}\left(\Omega r^{\beta/2}\right) + \left(k_4 - n\beta - 2v_o\left[\frac{r}{b}\right]^{\beta}\right) J_n\left(\Omega r^{\beta/2}\right)\right\} \right.$$
$$\left. + C_2 \left\{ r^{\beta/2}\beta\Omega\, Y_{n-1}\left(\Omega r^{\beta/2}\right) + \left(k_4 - n\beta - 2v_o\left[\frac{r}{b}\right]^{\beta}\right) Y_n\left(\Omega r^{\beta/2}\right)\right\}\right]. \tag{23}$$

Following a similar vein, with the conditions $\sigma_r(a) = -P$, $\sigma_r(b) = 0$, arbitrary constants are obtained

$$C_1 = \frac{Pa^{(k_1-1)/2}Y_n\left(\Omega b^{\beta/2}\right)}{J_n\left(\Omega b^{\beta/2}\right) Y_n\left(\Omega a^{\beta/2}\right) - J_n\left(\Omega a^{\beta/2}\right) Y_n\left(\Omega b^{\beta/2}\right)}, \tag{24a}$$

$$C_2 = -\frac{Pa^{(k_1-1)/2}J_n\left(\Omega b^{\beta/2}\right)}{J_n\left(\Omega b^{\beta/2}\right) Y_n\left(\Omega a^{\beta/2}\right) - J_n\left(\Omega a^{\beta/2}\right) Y_n\left(\Omega b^{\beta/2}\right)}. \tag{24b}$$

Up to this point, k_2 terms has been a positive value. Yet, when it is negative, one obtains two more cases depending on whether n is integer or not.

Case 3: $k_2 < 0$ and n is a non-integer number

For the constrains we have, radial stress yields to

$$\sigma_r = r^{(1-k_1)/2} \left[C_1 I_n \left(\Omega r^{\beta/2} \right) + C_2 I_{-n} \left(\Omega r^{\beta/2} \right) \right]. \tag{25}$$

Herein, $I_n(\Omega r^{\beta/2})$ and $I_{-n}(\Omega r^{\beta/2})$ are the modified Bessel functions of the first kind of order n and -n respectively. In a similar way, n and Ω are introduced. The calculation of the order n remains the same to Equation (14) but Ω alters slightly

$$n = \frac{\sqrt{(k_1 - 1)^2 - 4k_3}}{\beta}, \quad \Omega = -i \frac{2\sqrt{k_2}}{\beta}. \tag{26}$$

The series form of $I_n(\Omega r^{\beta/2})$ is

$$I_n \left(\Omega r^{\beta/2} \right) = \sum_{m=0}^{\infty} \frac{1}{m! \Gamma(m+n+1)} \left[\frac{\Omega r^{\beta/2}}{2} \right]^{2m+n}, \tag{27}$$

and $I_{-n}(\Omega r^{\beta/2})$ is achieved by inserting -n into the place of n in the above summation. Following a similar process to the previous cases, but this time operating with Equation (25), tangential stress and radial displacement equations are exhibited

$$\sigma_\theta = \frac{r^{(1-k_1)/2}}{2} \left[C_1 \left\{ r^{\beta/2} \beta \Omega I_{n-1} \left(\Omega r^{\beta/2} \right) + (k_4 - n\beta) I_n \left(\Omega r^{\beta/2} \right) \right\} + C_2 \left\{ r^{\beta/2} \beta \Omega I_{-n-1} \left(\Omega r^{\beta/2} \right) + (k_4 + n\beta) I_{-n} \left(\Omega r^{\beta/2} \right) \right\} \right], \tag{28}$$

$$u = \frac{r^{(3-k_1)/2}}{2E_o} \left[\frac{r}{b} \right]^{-\alpha} \left[C_1 \left\{ r^{\beta/2} \beta \Omega \, I_{n-1} \left(\Omega r^{\beta/2} \right) + \left(k_4 - n\beta - 2v_o \left[\frac{r}{b} \right]^\beta \right) I_n \left(\Omega r^{\beta/2} \right) \right\} \right.$$
$$\left. + C_2 \left\{ r^{\beta/2} \beta \Omega \, I_{-n-1} \left(\Omega r^{\beta/2} \right) + \left(k_4 + n\beta - 2v_o \left[\frac{r}{b} \right]^\beta \right) I_{-n} \left(\Omega r^{\beta/2} \right) \right\} \right]. \tag{29}$$

The closed forms of the arbitrary constants are

$$C_1 = -\frac{Pa^{(k_1-1)/2} I_{-n} \left(\Omega b^{\beta/2} \right)}{I_{-n} \left(\Omega b^{\beta/2} \right) I_n \left(\Omega a^{\beta/2} \right) - I_{-n} \left(\Omega a^{\beta/2} \right) I_n \left(\Omega b^{\beta/2} \right)}, \tag{30a}$$

$$C_2 = \frac{Pa^{(k_1-1)/2} I_n \left(\Omega b^{\beta/2} \right)}{I_{-n} \left(\Omega b^{\beta/2} \right) I_n \left(\Omega a^{\beta/2} \right) - I_{-n} \left(\Omega a^{\beta/2} \right) I_n \left(\Omega b^{\beta/2} \right)}. \tag{30b}$$

Due to non-integer n, $I_n(\Omega r^{\beta/2})$ and $I_{-n}(\Omega r^{\beta/2})$ are linearly independent solutions to the radial stress function. If n is an arbitrary integer number, the solution becomes the subsequent case.

Case 4: $k_2 < 0$ and n is an integer number

Under the given conditions, solution of the governing differential equation results in

$$\sigma_r = r^{(1-k_1)/2} \left[C_1 I_n \left(\Omega r^{\beta/2} \right) + C_2 K_n \left(\Omega r^{\beta/2} \right) \right]. \tag{31}$$

Hereinabove, $K_n(\Omega r^{\beta/2})$ is the modified Bessel function of the second kind of order n. The n and Ω are equal to the expressions in Equation (26). Moreover, $K_n(\Omega r^{\beta/2})$ can be connected to $I_n(\Omega r^{\beta/2})$ with the subsequent equation

$$K_n \left(\Omega r^{\beta/2} \right) = \frac{\pi}{2} \frac{I_{-n} \left(\Omega r^{\beta/2} \right) - I_n \left(\Omega r^{\beta/2} \right)}{\sin(n\pi)}. \tag{32}$$

Following a similar fashion to the previous cases, therein using Equation (31), tangential stress, radial displacement, and arbitrary constants are found.

$$\sigma_\theta = \frac{r^{(1-k_1)/2}}{2} \left[C_1 \left\{ r^{\beta/2} \beta \Omega I_{n-1} \left(\Omega r^{\beta/2} \right) + (k_4 - n\beta) I_n \left(\Omega r^{\beta/2} \right) \right\} \right.$$
$$\left. + C_2 \left\{ -r^{\beta/2} \beta \Omega K_{n-1} \left(\Omega r^{\beta/2} \right) + (k_4 - n\beta) K_n \left(\Omega r^{\beta/2} \right) \right\} \right], \tag{33}$$

$$u = \frac{r^{(3-k_1)/2}}{2E_o} \left[\frac{r}{b} \right]^{-\alpha} \left[C_1 \left\{ r^{\beta/2} \beta \Omega \, I_{n-1} \left(\Omega r^{\beta/2} \right) + \left(k_4 - n\beta - 2v_o \left[\frac{r}{b} \right]^\beta \right) I_n \left(\Omega r^{\beta/2} \right) \right\} \right.$$
$$\left. + C_2 \left\{ -r^{\beta/2} \beta \Omega \, K_{n-1} \left(\Omega r^{\beta/2} \right) + \left(k_4 - n\beta - 2v_o \left[\frac{r}{b} \right]^\beta \right) K_n \left(\Omega r^{\beta/2} \right) \right\} \right], \tag{34}$$

$$C_1 = \frac{Pa^{(k_1-1)/2} K_n \left(\Omega b^{\beta/2} \right)}{I_n \left(\Omega b^{\beta/2} \right) K_n \left(\Omega a^{\beta/2} \right) - I_n \left(\Omega a^{\beta/2} \right) K_n \left(\Omega b^{\beta/2} \right)}, \tag{35a}$$

$$C_2 = -\frac{Pa^{(k_1-1)/2} I_n \left(\Omega b^{\beta/2} \right)}{I_n \left(\Omega b^{\beta/2} \right) K_n \left(\Omega a^{\beta/2} \right) - I_n \left(\Omega a^{\beta/2} \right) K_n \left(\Omega b^{\beta/2} \right)}. \tag{36b}$$

Term k_2 has been either a positive or negative number to this stage. However, there is one more possibility which is the following:

Case 5: $k_2 = 0$

Let's take a deeper look into k_2 which is equal to $k_2 = v_o \, b^{-\beta}(g + \alpha - \beta)$. In this expression, v_o is the reference Poisson's ratio and b is the outer radius of the disk. Neither of them can be zero. Thus, in order for $k_2 = 0$ to happen, $g + \alpha - \beta$ term must be equal to zero. Moreover, this occurrence causes a change in the solution procedure of the governing differential equation. The governing equation reduces to

$$r^2 \frac{d^2\sigma_r}{dr^2} + k_1 r \frac{d\sigma_r}{dr} + k_3 \, \sigma_r = 0. \tag{36}$$

This equation is a second order homogeneous Cauchy-Euler type. Solving this equation gives the following radial stress function

$$\sigma_r = C_1 \, r^{(1-k_1-\sqrt{(k_1-1)^2-4k_3})/2} + C_2 r^{(1-k_1+\sqrt{(k_1-1)^2-4k_3})/2}. \tag{37}$$

Substituting Equations (3) and (37) into (9) provides the tangential stress

$$\sigma_\theta = C_1 \frac{k_4 - \sqrt{(k_1-1)^2 - 4k_3}}{2} r^{(1-k_1-\sqrt{(k_1-1)^2-4k_3})/2} + C_2 \frac{k_4 + \sqrt{(k_1-1)^2 - 4k_3}}{2} r^{(1-k_1+\sqrt{(k_1-1)^2-4k_3})/2}. \tag{38}$$

A straightforward combination of Equations (1)–(3), (10) and (37) renders to

$$u = \frac{1}{2E_o} \left[\frac{r}{b} \right]^{-\alpha} \left[C_1 \left(k_4 - \sqrt{(k_1-1)^2 - 4k_3} - 2v_o \left[\frac{r}{b} \right]^\beta \right) r^{(3-k_1-\sqrt{(k_1-1)^2-4k_3})/2} \right.$$
$$\left. + C_2 \left(k_4 + \sqrt{(k_1-1)^2 - 4k_3} - 2v_o \left[\frac{r}{b} \right]^\beta \right) r^{(3-k_1+\sqrt{(k_1-1)^2-4k_3})/2} \right]. \tag{39}$$

TABLE 1 Analytical solution methods to be followed based on parameters k_1, k_2 and k_3.

Constrains	Solution method
$k_1 = 0$	Depending on k_2 and n, among Cases 1–4, one of them occurs
$k_2 = 0$	Case 5
$k_3 = 0$	Depending on k_2 and n, among Cases 1–4, one of them occurs
$k_1 = k_2 = 0$	Appendix Case A.1
$k_1 = k_3 = 0$	Appendix Case A.2, this case in not possible for real numbers of α.
$k_2 = k_3 = 0$	Appendix Case A.3
$k_1 = k_2 = k_3 = 0$	Appendix Case A.4, this case in not possible for real numbers of α.

Solving Equation (37) for the internal pressure case boundary conditions, one acquires

$$C_1 = \frac{Pa^{\left(k_1 - 1 + \sqrt{(k_1-1)^2 - 4k_3}\right)/2} b^{\sqrt{(k_1-1)^2 - 4k_3}}}{a^{\sqrt{(k_1-1)^2 - 4k_3}} - b^{\sqrt{(k_1-1)^2 - 4k_3}}} , \tag{40a}$$

$$C_2 = -\frac{Pa^{\left(k_1 - 1 + \sqrt{(k_1-1)^2 - 4k_3}\right)/2}}{a^{\sqrt{(k_1-1)^2 - 4k_3}} - b^{\sqrt{(k_1-1)^2 - 4k_3}}}. \tag{40b}$$

As can be seen, the solution revolves around the parameter k_2. It can significantly alter the procedures to be followed. This situation has led us to examine the importance of other parameters (k_1, k_3) as well. Therefore, other conditions that could be critical such as $k_1 = 0$ or $k_3 = 0$ are investigated. It has been observed that some of these conditions may change the solution procedure slightly but not as much as k_2. Moreover, for instance, the case $k_1 = k_3 = 0$ is not possible for real values of α. In order to keep the conciseness of this research, these mathematically possible but quite rare cases are given in the Appendix section. Also, the necessary solution techniques are presented in Table 1 for a clearer understandability. After these elaborations, there is one possibility left, which is $\beta = 0$. When this occurs the term r^β in the governing equation becomes one and the differential equation's last term turns out as $k_2 + k_3$. The solution of this case is highly similar to Case 5. Furthermore, from an engineering point, $\beta = 0$ means that the Poisson's ratio does not vary along direction r. This is a case we frequently observe in the literature, which is taken into account in the articles to simplify the solution methods, see ref. [3, 5, 15, 42]. It reduces the problem to a classical Cauchy-Euler type equation. Yet, these simplifications result in some accuracy issues which we are going to discuss in the numerical examples.

In this study, further to stress and displacement functions, elastic limits of the stresses are also considered. The von Mises yield criterion (σ_{vm}) is utilized for this purpose

$$\sigma_{vm} = \sqrt{\sigma_r^2 - \sigma_r \sigma_\theta + \sigma_\theta^2} = \sigma_y, \tag{41}$$

in which σ_y is the yield strength of the material. Furthermore, in the subsequent numerical examples, unless otherwise stated the following dimensionless expressions are used

$$\bar{\sigma}_{vm} = \frac{\sigma_{vm}}{\sigma_y} , \bar{\sigma}_r = \frac{\sigma_r}{\sigma_y} , \bar{\sigma}_\theta = \frac{\sigma_\theta}{\sigma_y} , \bar{u} = \frac{uE_o}{b\sigma_y} , \bar{r} = \frac{r}{b} , \bar{P} = \frac{P}{\sigma_y} . \tag{42}$$

Hereabove, the overbar symbol denotes the dimensionless normalized quantities.

3 | NUMERICAL EXAMPLES

Before getting into the numerical examples, we would like to exhibit the preciseness of the analytical model. For this reason, our results are compared with a related study [43]. In that reference, the author has taken the Young's modulus as $E(r) = E_o (r/a)^\alpha$. Therefore, Equation (1) is swapped with this identity and the subsequent dimensionless terms

TABLE 2 Comparison of the dimensionless stresses and radial displacements.

| | $\bar{\sigma}_r$ | | | $\bar{\sigma}_\theta$ | | | $\bar{u}$ | | |
$\bar{r}$	**Present**	**Ref. [43]**	**% Difference**	**Present**	**Ref. [43]**	**% Difference**	**Present**	**Ref. [43]**	**% Difference**
0.6	−1.	−1.	0	2.9217569	2.9215247	−0.0079479	1.9330541	1.9329148	−0.0072067
0.7	−0.5193136	−0.5193327	0.0036778	1.9109654	1.9109177	−0.0024961	1.7741597	1.7738076	−0.0198599
0.8	−0.2542305	−0.2542463	0.0062144	1.3419100	1.3419577	0.0035545	1.6600641	1.6597794	−0.0171529
0.9	−0.0975499	−0.0975569	0.0071753	0.9966404	0.9967111	0.0070933	1.5784954	1.5784672	−0.0017865
1.0	0.	0.	0	0.7745855	0.7746334	0.0061835	1.5217854	1.5221546	0.0242551

are used:

$$\bar{\sigma}_r = \frac{\sigma_r}{\rho\omega^2 b^2 + P} \ , \bar{\sigma}_\theta = \frac{\sigma_\theta}{\rho\omega^2 b^2 + P} \ , \ \bar{u} = \frac{uE_o}{\rho\omega^2 b^3 + bP} \ , \ \bar{r} = \frac{r}{b} \ , \tag{43}$$

in which ρ and ω denote density and angular velocity. In order to be consistent with the reference, we used the above dimensionless terms in the verification procedure instead of Equation (42). The verification is made with the following reference values: E_o= 393 GPa, α = −1.322, v_o= 0.30, β = 0.01, a/b = 0.6, ω = 0, g = 0. In ref. [43], the researcher has preferred the usual constant Poisson's approach (β = 0). In the verification procedure, if β is set to be zero, we obtain an identical analytical solution to the reference (Cauchy-Euler type). However, our purpose is testing the Bessel function approach presented herein. In the case of setting β = 0, the order of the Bessel function n becomes indefinite, see Equations (15) and (26). For the purpose of avoiding this issue, we used a small number β = 0.01 which is close enough to zero. Following these arrangements, compared results are noted in Table 2. As can be seen from the table, we obtained highly closed numerical results by selecting β = 0.01. If β is chosen to be a number much closer to zero such as 0.000001, the less than 1% difference between the compared results gets even smaller. However, assign a number with this many digits to β considerably increases the computation time. Since the values at the table are almost perfectly matching with small fractional differences at the thousandths digit, it can be expressed that the constructed methods in this study are convenient. The percentage differences between computed stresses and displacements can be seen in the table as well. In these differences, we have simply used 100*(Reference-This study)/Reference formulation. Another interpretation comes to the surface from this comparison, and that is, if correct values are assigned to Bessel type equations, then one may get close enough solutions to Cauchy-Euler type equations as well. After this validation, we may begin numerical examples.

In this section, based on the numerical samples, stress and displacement fields are going to be analyzed from different perspectives. The following reference values are used throughout the examples: E_o= 300 GPa, σ_y= 400 MPa, v_o= 0.25, a/b = 0.5 and the dimensionless quantities in Equation (42) are utilized. We would like to state some points about the reference values. For instance, a/b ratio should be less than one since b > a. Poisson's ratio is selected as 0.25 because it varies within 0 to 0.5 for most materials. The numbers assigned for the Young's modulus and yield strength are generic values. Unless a specific material type is indicated, it is convenient to use these reference values. In the case of particular material selection then its properties must be followed. After these clarifications, firstly, we shall examine the effect of the geometry of the disk on the mentioned stress fields. The profile of the variable thickness disk is manipulated with the geometric parameter g. The component is investigated at the elastic limits for various values of g. Accordingly, the dimensionless von Mises stress variation along radius is stated in Figure 2a. When $\bar{\sigma}_{vm} = 1$, yielding commences at the internally pressurized disk. It is sufficient to look at Equation (41) to grasp the reason for this. If both sides of the equation are divided by σ_y, the right-hand side of the equation becomes 1. Additionally, $\bar{\sigma}_{vm}$ was previously determined as $\bar{\sigma}_{vm} = \sigma_{vm} /\sigma_y$. Thus, when the stress variation goes to 1, one may say the disk reaches its elastic limits. It is monitored from the figure that the disk geometry yields at its inner radius for different thickness profiles. Yet, the critical question to be asked here is whether this is always the case. The answer to this question is simply 'no'. The disk may yield at different positions. This topic is going to be later discussed in further details. When the disk thickness transitions from convex (g < 0) to concave (g > 0), the yield stresses in the figure tend to decrease along the radius. Moreover, for g equals to −1, −0.5, 0, 0.5 and 1, the calculated elastic limit internal pressure ($\bar{P}$) values are 0.42314, 0.46942, 0.51915, 0.57129, and 0.62444 respectively. In Figure 2b, the corresponding radial stresses are presented. At the elastic limits, since the distributions have negative values, these stress components are compressive. Also, at the inner radius, due to the boundary condition $\sigma_r(a) = -P$, these components are equal to $\bar{P}$ for each g value. It is observed by the figure that the thickness of the disk slightly changes the stresses in direction r. Followingly, in Figure 2c, the tangential stresses are exhibited. This figure shows highly
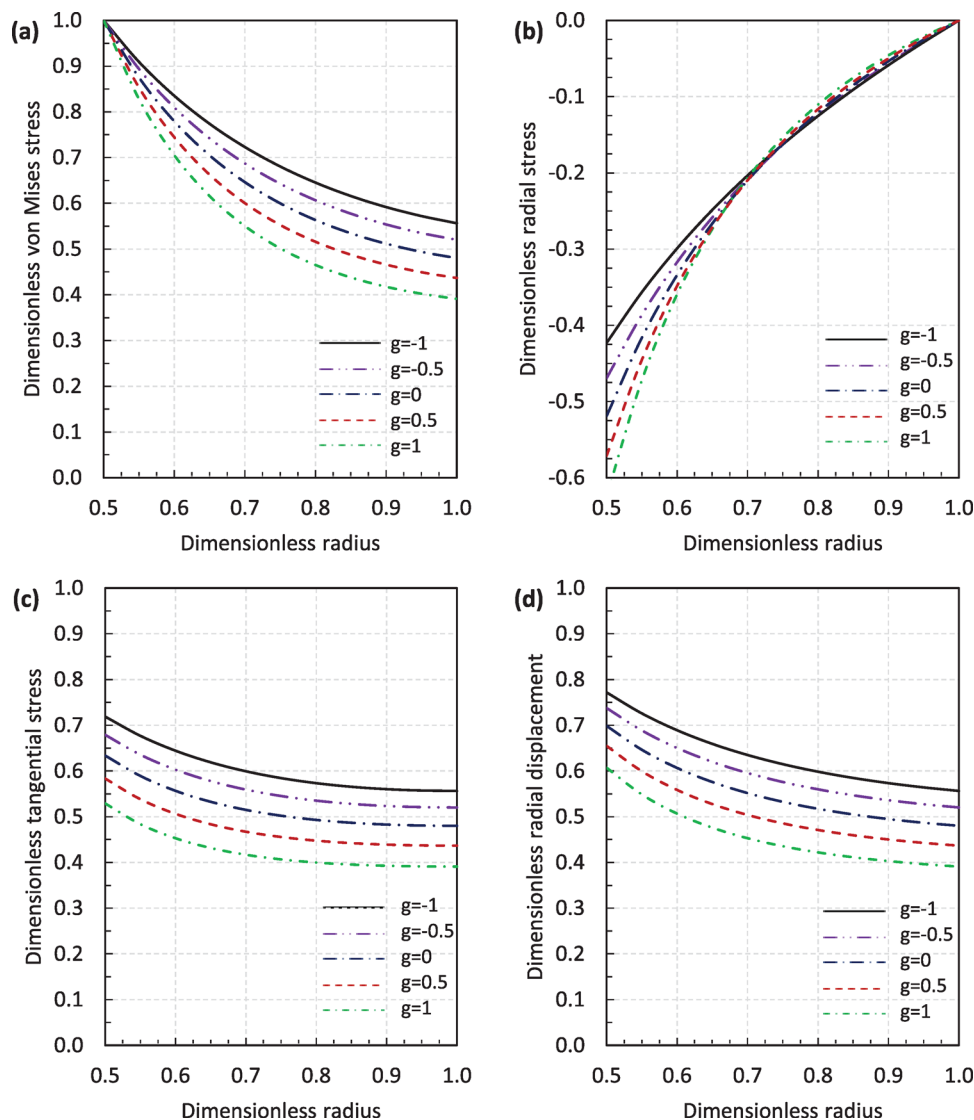
FIGURE 2 Effect of parameter g on (a) von Mises, (b) radial, (c) tangential stresses, and (d) radial displacement, where $\alpha = \beta = 1$.

resembling distributions with the von Mises stress. Since the von Mises stress is the combination of radial and tangential stress components and the magnitudes of the tangential stresses are greater than the radial ones, the resemblance is unsurprising. Contrary to radial stresses, tangential ones are tensile. In the last constituent, radial displacements are given in Figure 2d. Applying limit internal pressure to the disk results in radial expansion. This expansion is higher for the disk with convex profile.

The material grading parameters (α, β) have been kept constant in the previous analysis. Here, we continue with the convex disk profile (g = −0.5) and examine the grading parameters by altering them. Let's begin with parameter α. In Figure 3a, von Mises stress distributions are illustrated for various α values. Once again, yielding occurs at the inner radius. As the values of α increase, the stress distributions tend to get lower through radial positions closer to the outer radius. The limit pressure values are obtained as 0.30939, 0.34302, 0.38092, 0.42314, and 0,46942 for α −1, −0.5, 0, 0.5 and 1 respectively. In the next step, in Figure 3b, radial stresses are displayed. Comparing this figure with the previous radial stress figure, Figure 2b, reveals that g and α may cause different stress distribution profiles. At the elastic limits, even though in both cases these distributions are compressive, their variations along the disk radius are considerably different. From this outcome, another interpretation can be made as well. Since it is hard to manipulate the material properties in realistic engineering cases, in order to achieve the desired stress field, one should attempt to change the disk geometry instead. In the ensuing Figure 3c tangential stresses are observed for various α values. Once again, this component and the von Mises stress are tensile and similar to each other. In this stress direction, small modifications in parameter α may
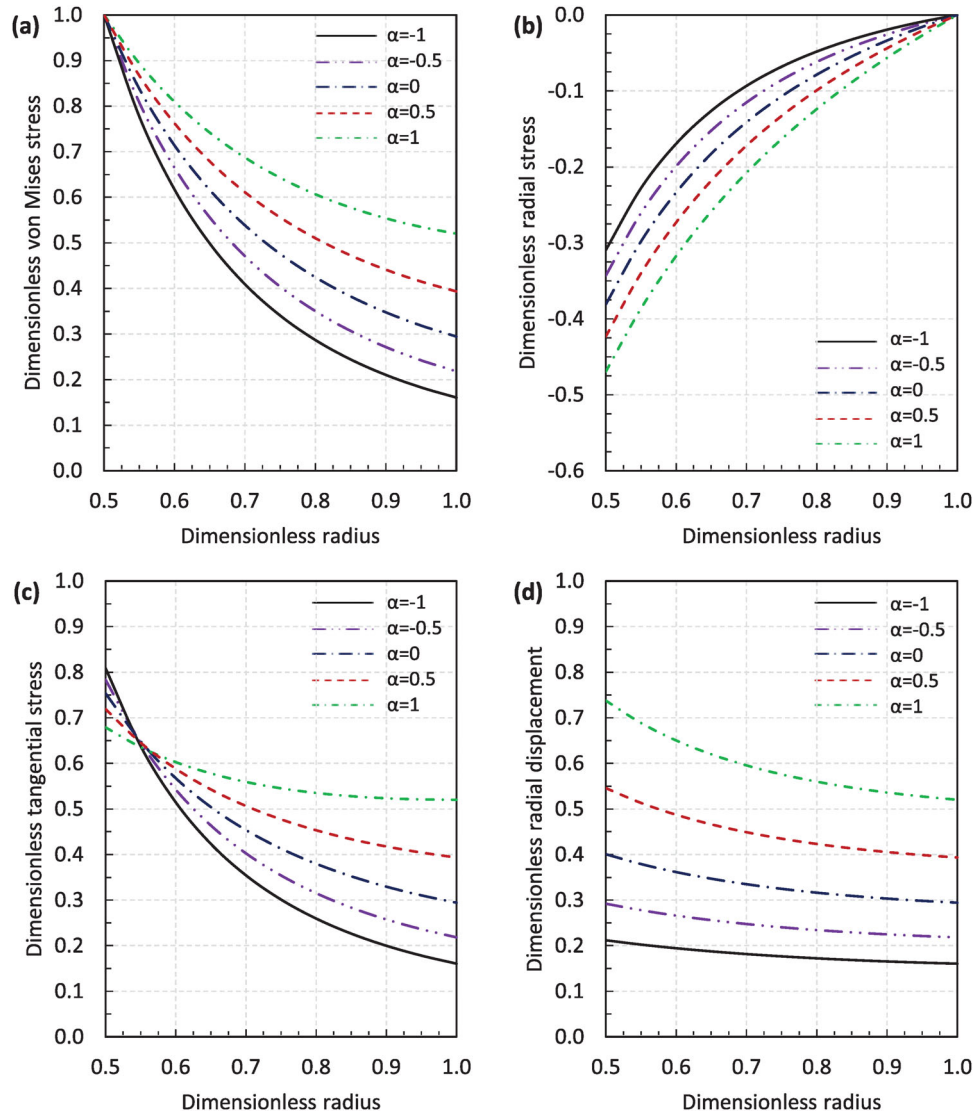
FIGURE 3 Effect of parameter α on (a) von Mises, (b) radial, (c) tangential stresses, and (d) radial displacement, where $\beta = 1$, g $= -0.5$.

result in prominent stress magnitude differences. In order to perceive this, the stress differences between the inner and outer radius of the disk can be checked. In the last constituent, Figure 3d, radial displacements are illustrated. Altering parameter α immensely changes the magnitude of the radial displacement. Thus, it is important to state that for cases where the displacement is a priority in the mechanical design of such components, grading of the Young's modulus should be paid attention to.

In the next examination, the effect of grading parameter β is focused on. Herein, Young's modulus grading parameter ($\alpha = 1$) and geometric parameter (g $= -0.5$) are kept constant. Stress and displacement fields are investigated for different β values. For β -0.99, -0.5, 0, 0.5 and 1, limit pressures are computed as 0.50261, 0.48759, 0.47813, 0.47268, and 0.46942 respectively. As can be seen from the constituents of Figure 4, directional stresses and radial displacement moderately change with parameter β. It is apparent that parameters α and g have much more importance than β. Therefore, as far as we know, almost all similar studies in the literature have taken Poisson's ratio as constant or in other words $\beta = 0$. This consideration delivers both positive and negative consequences. On the one hand, in terms of mathematical modeling, the problem turns out as a simple Cauchy-Euler type when $\beta = 0$. So, the solution technique can be handled without much effort. On the other hand, this consideration causes accuracy problems. When all parts of Figure 4 are examined, it is apparent that parameter β influences both the stresses and displacement to some degree. Since including the effect of parameter β in the analytical model of the problem is not a simple task, variable Poisson's ratio has been avoided in the
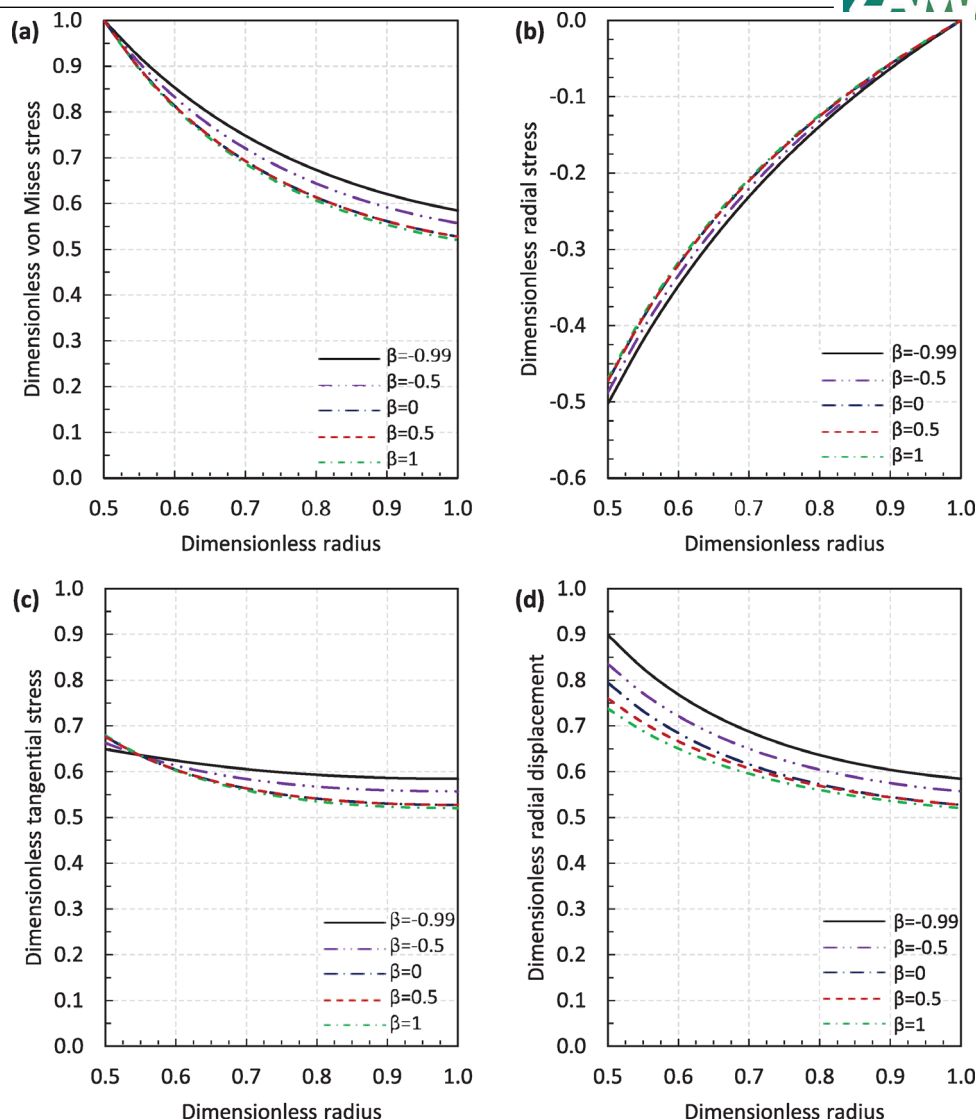
FIGURE 4 Effect of parameter β on (a) von Mises, (b) radial, (c) tangential stresses, and (d) radial displacement, where $\alpha = 1$, g $= -0.5$.

scientific literature for the power-law graded disk. Therefore, the fact that parameter β is assigned as a variable is related to how precise the study is. If variable Poisson's ratio path is followed, there emerges a technical matter to be considered when assigning values to β. As known Poisson's ratio varies between 0 and 1/2 for most materials. In order not to pass these boundaries, Equation (2) should be solved within this range. For the reference values in the numerical examples ($v_o =$ 0.25, $a/b = 0.5$), if $0 < v(r) < 1/2$ inequality is solved, one finds that β must be greater than -1. Therefore, for mathematical correctness purposes, in Figure 4, -0.99 is assigned to β instead of -1. If β is equal to -1 then $v(r)$ becomes 1/2 at the inner radius of the disk. For β values smaller than -1, $v(r)$ pass 1/2 and this may cause incorrect interpretations. Moreover, in ref. [3], the inequality for $v(r)$ has been taken with a slight boundary difference as $0 \leq v(r) < 1/2$. It is true that for some materials such as cork, Poisson's ratio could be equal to zero. However, if Equation (2) is considered, having a boundary equal to zero is not likely. In this study, $v(r) = v_o (r/b)^\beta$, and for $v(r)$ to be zero, reference Poisson's ratio (v_o) must be equal to zero since $(r/b)^\beta$ term cannot be zero due to the geometry. If there is no inner hole in the disk ($a = 0$), $(r/b)^\beta$ term can be equal to zero when r $= a$. However, the geometry of the disk contains an inner hole ($a \neq 0$), this possibility is disregarded, see Figure 1. Under these circumstances, one may conclude that having a variable Poisson's ratio brings both analytical and numerical difficulty to the investigation while increasing the accuracy. When $\beta = 0$ case is taken as reference point then compared with high and low β values, 1 and -0.99, we have observed around 3% to 9% differences in the distributions of all figure constituents of Figure 4. While β is a positive value, distribution differences are towards the smaller side. However, in the case of negative values of β, differences in the distributions tend to rise. As a concluding remark,
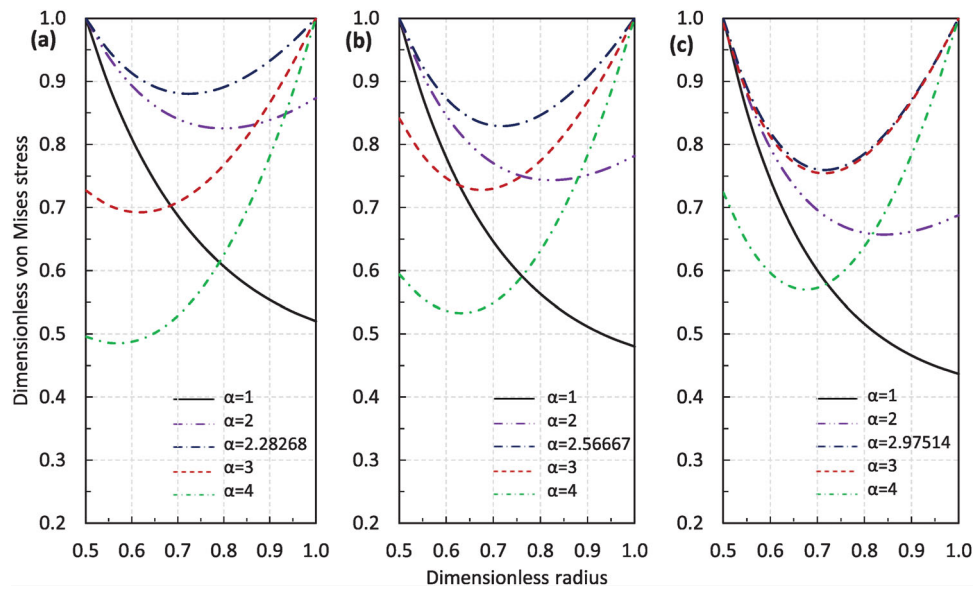
FIGURE 5 Location of the disk yielding commencement for various disk thickness profiles and α values, where $\beta = 1$ and at (a) $g = -0.5$, (b) $g = 0$, and (c) $g = 0.5$.
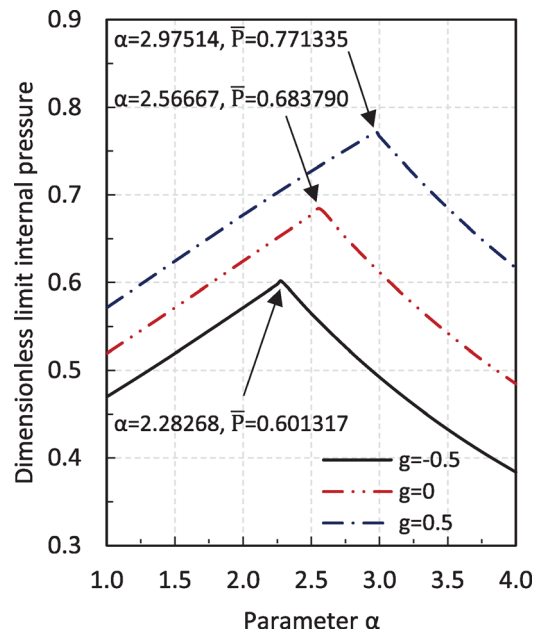

FIGURE 6 Dimensionless limit internal pressure alteration for various α and g parameters, where $\beta = 1$.

depending on the value of β, roughly around 10% increase in the predicted results with the variable β consideration can be observed.

We have investigated the material and geometric parameters to this point. Let's switch our focal point to yielding and its position. At the beginning of the numerical examples, it has been mentioned that yielding may occur at different locations. According to the von Mises criterion, yielding can commence at the inner radius, outer radius, or both simultaneously. For disk of convex ($g = -0.5$), annular ($g = 0$) and concave ($g = 0.5$) profiles, all these yielding positions are possible for different α values. The von Mises stress distributions of these disk profiles are given in Figure 5. Whilst searching for yielding positions, an interesting topic has been noticed. When the disk yields at the inner and outer radius at the same time, the highest possible pressure values are reached. Thus, the α value at this point is called critical α (α_{cr}). In order to illustrate this, Figure 6 is plotted for the same disk geometries used in the last figure. Prior to or after α_{cr}, limit
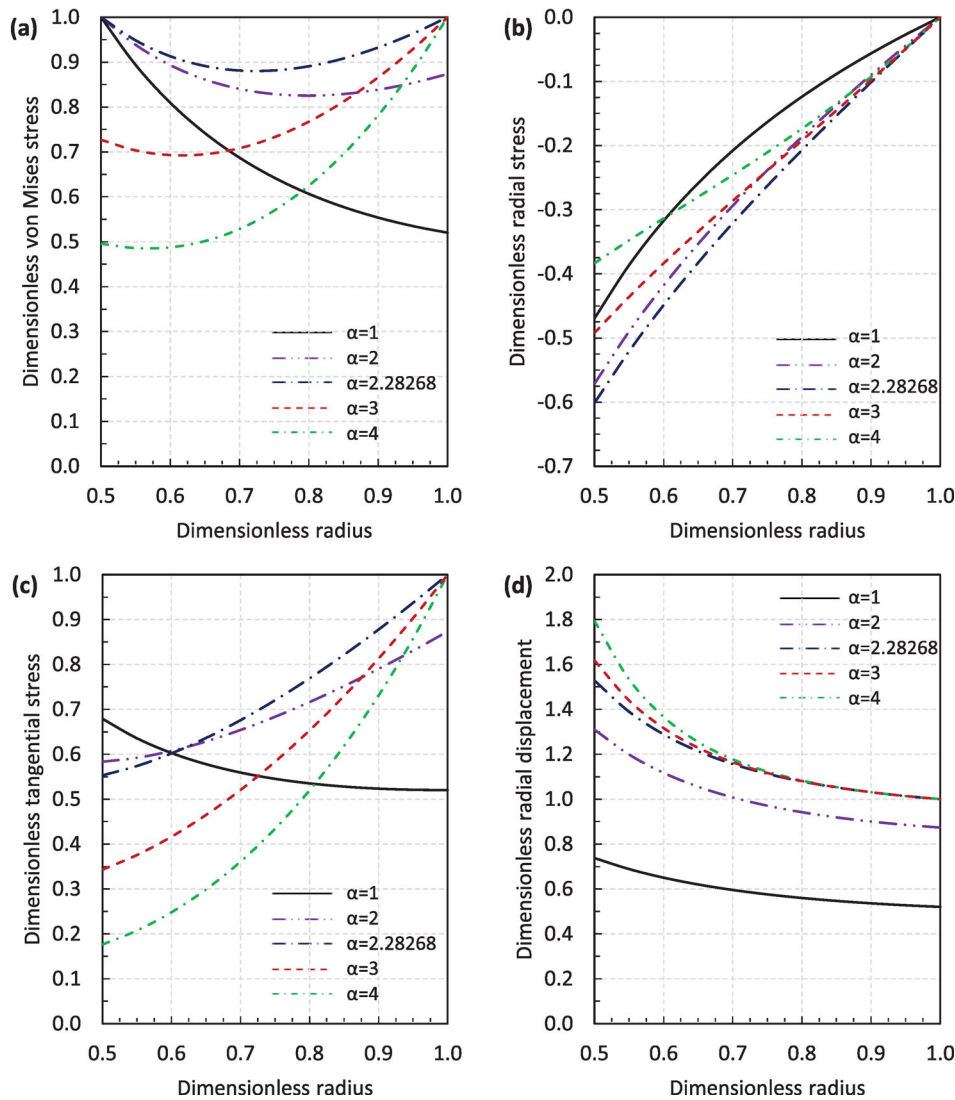
FIGURE 7 Dimensionless (a) von Mises, (b) radial, (c) tangential stresses, and (d) radial displacement for different α values before, at, and after critical level, where $\beta = 1$, g $= -0.5$.

internal pressures are considerably lower than at α_{cr}. For this reason, one may interpret that if higher limit pressures are the priority in the design of such structural elements, one should pay attention to these critical values. Let's return to the previous analyses of g, α, and β. Therein these exemplifying figures, all values of α are values smaller than α_{cr}. Therefore, we decided to investigate stress and displacement fields at α_{cr} and after α_{cr} values. Constituents of Figure 7 serve this purpose. Wherein g $= -0.5$ and $\beta = 1$, and for α 1, 2, 2.28268, 3, and 4, limit pressures are found as 0.46942, 0.57129, 0.60132, 0.49214, and 0.38343. In Figure 7a, one observes different yielding positions. For α values smaller than α_{cr}, the disk yields at the inner radius. When $\alpha =\alpha_{cr}$, disk yields at the inner and outer radius simultaneously. When α is greater than α_{cr}, disk tends to yield at the outer radius. Depending on the values of α, stress distribution of the von Mises stress highly alters. In Figure 7b, the highest-pressure magnitude at the inner radius is observed for the disk with α_{cr} value. Moreover, if this figure and Figure 3b are compared, one can see that before and after the critical value of α, the curvature of the stress distribution profiles alters. In Figure 7c, the corresponding tangential stresses are demonstrated. Therefrom the figure, obvious differences in the stress distribution profiles can be easily identified. Hence, we can, without a doubt, state that α_{cr} is a noticeably important parameter at the elastic limits. In the final constituent, Figure 7d, radial displacements are illustrated. Herein, under this mechanical load, disk radially expands. For higher values of α, this expansion increases. Nevertheless, at some point, the degree of this expansion reduces especially for values greater than α_{cr}.

To this point in the research, all numerical examples have been displayed for the disk at the elastic limits. In the final example, before closure, we would like to demonstrate a case where the disk is arbitrarily loaded below the limits. Wherein,
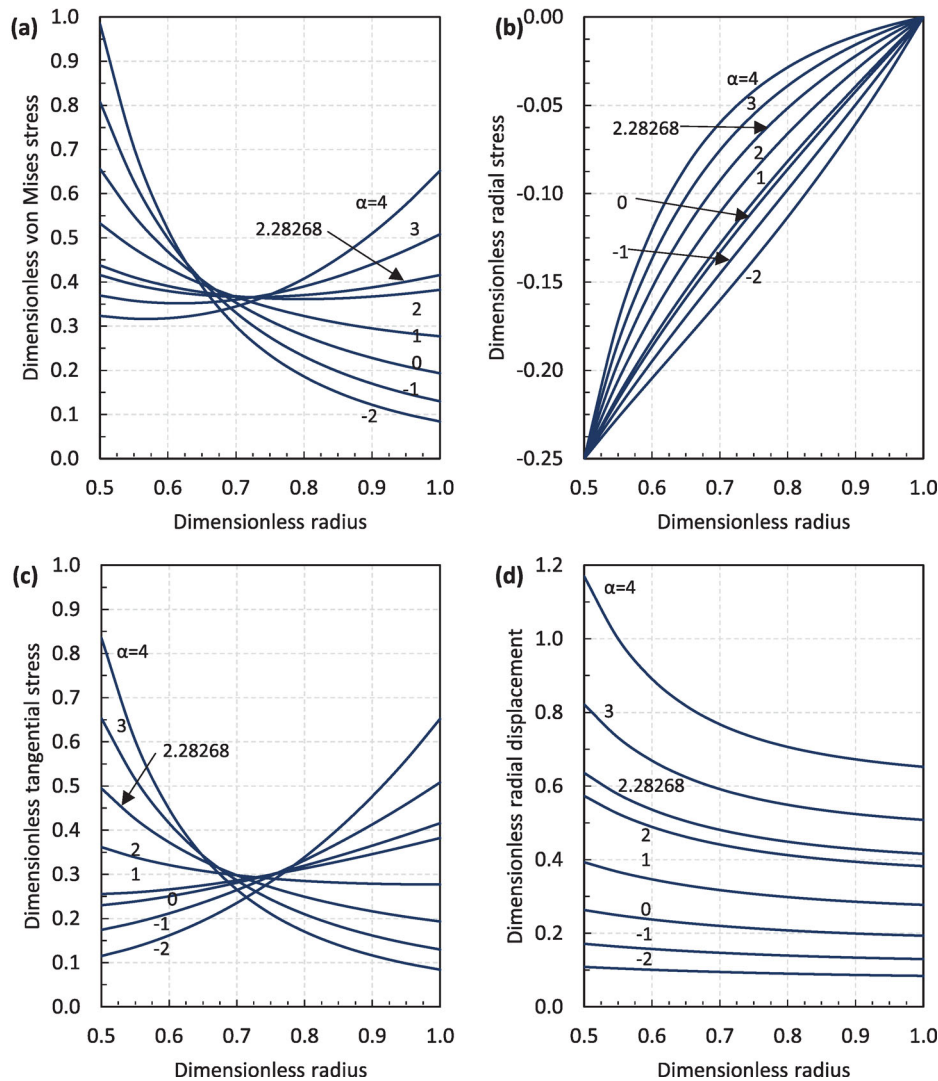
FIGURE 8 Dimensionless (a) von Mises, (b) radial, (c) tangential stresses, and (d) radial displacement for different α, where the disk is subjected to an arbitrary internal pressure, $\bar{P} = 0.25$.

once again, the common parameters g = −0.5 and β = 1 are selected. The applied pressure load is kept constant, $\bar{P}$= 0.25, and α is altered. In Figure 8a, none of the von Mises distributions reach to 1, so the disk is loaded below the limits, just the case $\alpha = -2$ gets closer to its limit. When the figure and Figure 7a are compared for α 1, 2, 2.28268, 3, and 4, one can visually identify that stress variation profiles change to some extent according to the magnitude of the applied load. Also, this interpretation is valid for the radial and tangential stresses in Figure 8b,c if these figures are compared with the corresponding Figure 7b,c. Additionally, the comparison of Figures 7d and 8d for α 1, 2, 2.28268, 3, and 4 reveals that the magnitude of the applied pressure highly influences the elastic radial displacement magnitudes. Furthermore, one may reach to another outcome: α_{cr} is an important parameter at or near limit loads since α_{cr} does not make a significant change in the components of Figure 8.

4 | CONCLUDING REMARKS

Disks are important components used vastly in different engineering sectors. In this examination, the elastic solution of the power-law functionally graded variable thickness disk is investigated with analytical methods. Depending on the parameters, the solution mostly yields Bessel type functions but occasionally one may deal with Cauchy-Euler type equations as well. In instances where Bessel functions occur, Case 1 and Case 3 are the ones we solve since the order of the

Bessel function is non-integer for most possibilities. Mathematically infrequent cases are shown in the appendix as well. After analytical procedures, in the numerical examples, some important details were found:

1. Parameter g can be used to control the desired stress field. In engineering component design, it is easier to alter the geometry while physically manufacturing the disk than to alter material grading parameters.
2. Overall, grading parameter α is the most significant parameter since it prominently affects both stresses and displacements. If the component is used at or close to the limit loads, the grading of the material should be as close as possible to α_{cr}.
3. The grading parameter β is the most neglected parameter in the design of power-law functionally graded disk components. It is true that including this parameter in the problem brings a significant amount of difficulty, yet, it rises the predicted accuracy. Therefore, this matter could be remarked as a finishing touch to a mechanical modeling. Depending on the value of β, differences between variable β and β = 0 cases change between 3 to 9% in the numerical examples. For different values, the mentioned difference may increase or decrease. So, from a general perspective, roughly around 10% increase in accuracy with variable β can be expected.
4. The cases that are shown in the Appendix have not been revealed before due to the absence of parameter β consideration. From a mathematical perspective, these singular cases should be handled carefully to have correct closed-form solutions.
5. Bringing parameter β into the problem has broadened the available analytical solution methods. In this way, instead of the classical Cauchy-Euler type differential equation solutions, one may utilize Bessel-type functions as well. It should be expressed that for different grading rules that include variable Poisson's ratio approach, closed-form solutions may not always be reached.
6. Although the results have been verified by comparison, analytical solutions can be extended with other appropriate numerical techniques as well.

Apart from the above remarks, the methods in this study can be further developed for different purposes including weight optimization or stress field optimization. The reason for pinpointing these topics is due to the importance of functionally graded material applications. In most engineering designs, standard isotropic materials like steel are utilized. In cases that need special attention functionally graded materials or other special counterpart materials are generally employed. In these special cases, weight or stress fields might be prioritized. Additionally, fatigue behavior of similar structures can be investigated by modeling with time dependency. Another option is above elastic limit load conditions such as elastic-plastic or fully plastic zones. These stress zones can be further investigated in future studies.

CONFLICT OF INTEREST STATEMENT
The authors declare that there is no conflict of interest.

REFERENCES

[1] Saleh, B., Jiang, J., Ma, A., Song, D., Yang, D., Xu, Q.: Review on the influence of different reinforcements on the microstructure and wear behavior of functionally graded aluminum matrix composites by centrifugal casting. Met. Mater. Int. 26, 933–960 (2020)

[2] Zhang, N., Khan, T., Guo, H., Shi, Z., Zhong, W., Zhang, W.: Functionally graded materials: an overview of stability, buckling, and free vibration analysis. Adv. Mater. Sci. Eng. 2019, 1354150 (2019)

[3] Horgan, C.O., Chan, A.M.: The pressurized hollow cylinder or disk problem for functionally graded isotropic linearly elastic materials. J. Elast. 55, 43–59 (1999)

[4] You, L.H., Wang, J.X., Tang, B.P.: Deformations and stresses in annular disks made of functionally graded materials subjected to internal and/or external pressure. Meccanica. 44, 283–292 (2009)

[5] Çallioğlu, H.: Stress analysis in a functionally graded disc under mechanical loads and a steady state temperature distribution. Sadhana. 36, 53–64 (2011)

[6] Nejad, M.Z., Abedi, M., Lotfian, M.H., Ghannad, M.: Elastic analysis of exponential fgm disks subjected to internal and external pressure. Cent. Eur. J. Eng. 3, 459–465 (2013)

[7] Eraslan, A.N., Akis, T.: Elastoplastic response of a long functionally graded tube subjected to internal pressure. Turkish J. Eng. Environ. Sci. 29, 361–368 (2005)

[8] Saeedi, S., Kholdi, M., Loghman, A., Ashrafi, A., Arefi, M.: Thermo-elasto-plastic analysis of thick-walled cylinder made of functionally graded materials using successive approximation method. Int. J. Press. Vessel. Pip. 194, 104481 (2021)

[9] Eraslan, A.N., Akis, T.: Plane strain analytical solutions for a functionally graded elastic–plastic pressurized tube. Int. J. Press. Vessel. Pip. 83, 635–644 (2006)

[10] Benslimane, A., Bouzidi, S., Methia, M.: Displacements and stresses in pressurized thick-walled fgm cylinders: exact and numerical solutions. Int. J. Press. Vessel. Pip. 168, 219–224 (2018)

[11] Sadrabadi, S.A., Rahimi, G.H., Citarella, R., Karami, J. S., Sepe, R., Esposito, R.: Analytical solutions for yield onset achievement in fgm thick walled cylindrical tubes undergoing thermomechanical loads. Compos. Part B-Eng. 116, 211–223 (2017)

[12] Benslimane, A., Medjdoub, C., Methia, M., et al.: Investigation of displacement and stress fields in pressurized thick-walled fgm cylinder under uniform magnetic field. Mater Today. Proc. 36, 101–106 (2021)

[13] Tutuncu, N., Ozturk, M.: Exact solutions for stresses in functionally graded pressure vessels. Compos. Part B-Eng. 32, 683–686 (2001)

[14] Nejad, M.Z., Alamzadeh, N. Hadi, A.: Thermoelastoplastic analysis of fgm rotating thick cylindrical pressure vessels in linear elastic-fully plastic condition. Compos. Part B-Eng. 154, 410–422 (2018)

[15] Kacar, I.: Exact elasticity solutions to rotating pressurized axisymmetric vessels made of functionally graded materials (fgm). Materialwiss. Werkstofftech. 51, 1481–1492 (2020)

[16] Anani, Y., Rahimi, G.H.: Stress analysis of thick pressure vessel composed of functionally graded incompressible hyperelastic materials. Int. J. Mech. Sci. 104, 1–7 (2015)

[17] Nayebi, A., Sadrabadi, S.A.: fgm elastoplastic analysis under thermomechanical loading. Int. J. Press. Vessel. Pip. 111, 12–20 (2013)

[18] Arslan, E., Mack, W., Apatay, T.: Thermo-mechanically loaded steel/aluminum functionally graded spherical containers and pressure vessels. Int. J. Press. Vessel. Pip. 191, 104334 (2021)

[19] Bayat, Y., Ghannad, M., Torabi, H.: Analytical and numerical analysis for the fgm thick sphere under combined pressure and temperature loading. Arch. Appl. Mech. 82, 229–242 (2012)

[20] Ahmadi, S.R., Sheikhlou, M., Gharebagh, V.M.: Thermo-elastic/plastic semi-analytical solution of incompressible functionally graded spherical pressure vessel under thermo-mechanical loading. Acta Mech. 222, 161–173 (2011)

[21] Tutuncu, N., Temel, B.: A novel approach to stress analysis of pressurized FGM cylinders, disks and spheres. Compos. Struct. 91, 385–390 (2009)

[22] Atashipour, S.A., Sburlati, R., Atashipour, S.R.: Elastic analysis of thick-walled pressurized spherical vessels coated with functionally graded materials. Meccanica. 49, 2965–2978 (2014)

[23] Wang, Z.W., Zhang, Q., Xia, L.Z., Wu, J. T., Liu, P. Q., Thermomechanical analysis of pressure vessels with functionally graded material coating. J. Press. Vessel. Technol. 138, 011205 (2016)

[24] Eraslan, A.N., Akis, T.: Analytical solutions to elastic functionally graded cylindrical and spherical pressure vessels. J. Multidiscip. Eng. Sci. Technol. 2, 2687–2693 (2015)

[25] Tutuncu, N.: Stresses in thick-walled fgm cylinders with exponentially-varying properties. Eng. Struct. 29, 2032–2035 (2007)

[26] Jabbari, M., Bahtui, A., Eslami, M.R.: Axisymmetric mechanical and thermal stresses in thick short length fgm cylinders. Int. J. Press. Vessel. Pip. 86, 296–306 (2009)

[27] Jabbari, M., Karampour, S., Eslami, M.R.: Steady state thermal and mechanical stresses of a poro-piezo-FGM hollow sphere. Meccanica. 48, 699–719 (2013)

[28] Hajisadeghian, A., Masoumi, A., Parvizi, A.: Analytical investigation of elastic and plastic behavior of rotating double-walled FGM-homogenous hollow shafts. Arch. Appl. Mech. 91, 1343–1369 (2021)

[29] Akis, T., Eraslan, A.N.: The stress response and onset of yield of rotating fgm hollow shafts. Acta Mech. 187, 169–187 (2006)

[30] Akis, T., Eraslan, A.N.: Exact solution of rotating fgm shaft problem in the elastoplastic state of stress. Arch. Appl. Mech. 77, 745–765 (2007)

[31] Heydarpour, Y., Malekzadeh, P., Haghighi, M.G., Vaghefi, M.: Thermoelastic analysis of rotating laminated functionally graded cylindrical shells using layerwise differential quadrature method. Acta Mech. 223, 81–93 (2012)

[32] Chen, J., Ding, H., Chen, W.: Three-dimensional analytical solution for a rotating disc of functionally graded materials with transverse isotropy. Arch. Appl. Mech. 77, 241–251 (2007)

[33] Durodola, J.F., Attia, O., Deformation and stresses in functionally graded rotating disks. Compos. Sci. Technol. 60, 987–995 (2000)

[34] Dai, T., Dai, H.L.: Thermo-elastic analysis of a functionally graded rotating hollow circular disk with variable thickness and angular speed. Appl. Math. Model. 40, 7689–7707 (2016)

[35] Zheng, Y., Bahaloo, H., Mousanezhad, D., Mahdi, E., Vaziri, A., Nayeb-Hashemi, H.: Stress analysis in functionally graded rotating disks with non-uniform thickness and variable angular velocity. Int. J. Mech. Sci. 119, 283–293 (2016)

[36] Bayat, M., Saleem, M., Sahari, B.B., Hamouda, A.M.S., Mahdi, E.: Analysis of functionally graded rotating disks with variable thickness. Mech. Res. Commun. 35, 283–309 (2008)

[37] Sondhi, L., Thawait, A.K., Sanyal, S., Bhowmick, S.: Stress and deformation analysis of functionally graded varying thickness profile orthotropic rotating disk. Mater. Today. Proc. 33, 5455–5460 (2020)

[38] Essa, S., Argeso, H.: Elastic analysis of variable profile and polar orthotropic FGM rotating disks for a variation function with three parameters. Acta Mech. 228, 3877–3899 (2017)

[39] Zafarmand, H., Hassani, B.: Analysis of two-dimensional functionally graded rotating thick disks with variable thickness. Acta Mech. 225, 453–464 (2014)

[40] Eldeeb, A.M., Shabana, Y.M., Elsawaf, A.: Influences of angular deceleration on the thermoelastoplastic behaviors of nonuniform thickness multilayer fgm discs. Compos. Struct. 258, 113092 (2021)

[41] Nayak, P., Bhowmick, S., Saha, K.N.: Elasto-plastic analysis of thermo-mechanically loaded functionally graded disks by an iterative variational method. Eng. Sci. Technol. Int. J. 23, 42–64 (2020)

[42] Çallioğlu, H., Sayer, M., Demir, E.: Elastic–plastic stress analysis of rotating functionally graded discs. Thin Walled Struct. 94, 38–44 (2015)

[43] Yıldırım, V.: The best grading pattern selection for the axisymmetric elastic response of pressurized inhomogeneous annular structures (sphere/cylinder/annulus) including rotation. J. Braz. Soc. Mech. Sci. Eng. 42, 1–19 (2020)

APPENDIX

The governing differential equation is given below

$$r^2 \frac{d^2\sigma_r}{dr^2} + k_1 r \frac{d\sigma_r}{dr} + \left[k_2 r^\beta + k_3 \right] \sigma_r = 0, \tag{A1}$$

where

$$k_1 = 3 + g - \alpha, \, k_2 = v_o \, b^{-\beta} (g + \alpha - \beta), \, k_3 = g(1 - \alpha) - \alpha. \tag{A2}$$

Case A.1 $k_1 = k_2 = 0$

For k_1 and k_2 to be equal to zero simultaneously, the following two conditions must occur

$$g = \alpha - 3, \, \beta = 2\alpha - 3. \tag{A3}$$

Under these circumstances, $k_1 = k_2 = 0$ and k_3 becomes

$$k_3 = -\alpha^2 + 3\alpha - 3. \tag{A4}$$

The governing equation simplifies to

$$r^2 \frac{d^2\sigma_r}{dr^2} + k_3 \, \sigma_r = 0, \tag{A5}$$

and the solutions are acquired as

$$\sigma_r = C_1 \, r^{\left(1 - \sqrt{1-4k_3}\right)/2} + C_2 r^{\left(1 + \sqrt{1-4k_3}\right)/2}, \tag{A6}$$

$$\sigma_\theta = C_1 \frac{1}{2} \left(3 + 2g - \sqrt{1 - 4k_3} \right) r^{\left(1 - \sqrt{1-4k_3}\right)/2} + C_2 \frac{1}{2} \left(3 + 2g + \sqrt{1 - 4k_3} \right) r^{\left(1 + \sqrt{1-4k_3}\right)/2}, \tag{A7}$$

$$u = \frac{1}{2E_o} \left[\frac{r}{b} \right]^{-\alpha} \left[C_1 \left\{ 3 + 2g - \sqrt{1 - 4k_3} - 2v_o \left[\frac{r}{b} \right]^\beta \right\} r^{\left(3 - \sqrt{1-4k_3}\right)/2} \right.$$

$$\left. + C_2 \left\{ 3 + 2g + \sqrt{1 - 4k_3} - 2v_o \left[\frac{r}{b} \right]^\beta \right\} r^{\left(3 + \sqrt{1-4k_3}\right)/2} \right]. \tag{A8}$$

Utilizing $\sigma_r(a) = -P$, $\sigma_r(b) = 0$, arbitrary constants are found

$$C_1 = \frac{Pa^{\left(\sqrt{1-4k_3}-1\right)/2}b^{\sqrt{1-4k_3}}}{a^{\sqrt{1-4k_3}} - b^{\sqrt{1-4k_3}}} \;,\; C_2 = -\frac{Pa^{\left(\sqrt{1-4k_3}-1\right)/2}}{a^{\sqrt{1-4k_3}} - b^{\sqrt{1-4k_3}}} \;. \tag{A9}$$

Case A.2 $k_1 = k_3 = 0$

In order for k_1 and k_3 to be equal to zero together, let's set the first and third constituent of (A2) to zero. What we end up is then

$$g = \alpha - 3, \; g = \frac{\alpha}{1-\alpha} \;. \tag{A10}$$

Accordingly, the geometric parameter g must satisfy the above conditions. Solving the condition for α, one finds

$$\alpha - 3 = \frac{\alpha}{1-\alpha} \rightarrow \alpha = \frac{1}{2}\left(3 \pm i\sqrt{3}\right). \tag{A11}$$

As can be seen, α turns out as imaginary number. This reveals that for a realistic mechanical modeling of the problem $k_1 = k_3 = 0$ cannot occur.

Case A.3 $k_2 = k_3 = 0$

In a similar way, second and third constituent of (A2) are set to zero to acquire the necessary constrains

$$g = \frac{\alpha}{1-\alpha} \;,\; \beta = \frac{\alpha(2-\alpha)}{1-\alpha} \;. \tag{A12}$$

If the above constrains are satisfied, $k_2 = k_3 = 0$ and k_1 happens to be

$$k_1 = 3 + \frac{\alpha^2}{1-\alpha}. \tag{A13}$$

The main equation is then

$$r^2\frac{d^2\sigma_r}{dr^2} + k_1 r \frac{d\sigma_r}{dr} = 0. \tag{A14}$$

Stress and displacement field functions are obtained as follows for the above equation

$$\sigma_r = C_1 \frac{1}{1-k_1}r^{1-k_1} + C_2, \tag{A15}$$

$$\sigma_\theta = C_1 \frac{2+g-k_1}{1-k_1}r^{1-k_1} + C_2(1+g), \tag{A16}$$

$$u = \frac{1}{E_o}\left[\frac{r}{b}\right]^{-\alpha}\left[C_1\frac{1}{1-k_1}\left\{2+g-k_1-v_o\left[\frac{r}{b}\right]^\beta\right\}r^{2-k_1} + C_2\left\{1+g-v_o\left[\frac{r}{b}\right]^\beta\right\}r\right], \tag{A17}$$

$$C_1 = \frac{P(1-k_1)a^{k_1}b^{k_1}}{a^{k_1}b - ab^{k_1}} \;,\; C_2 = -\frac{Pa^{k_1}b}{a^{k_1}b - ab^{k_1}}. \tag{A18}$$

Case A.4 $k_1 = k_2 = k_3 = 0$

For $k_1 = k_2 = k_3 = 0$ to happen, all constituents of (A2) are set to zero, and the following expressions are obtained

$$g = \alpha - 3, \; \beta = g + \alpha, \; g = \frac{\alpha}{1-\alpha} \;. \tag{A19}$$

From the first and the third component of the above conditions, we find the same results presented in (A11)

$$\alpha - 3 = \frac{\alpha}{1 - \alpha} \rightarrow \alpha = \frac{1}{2}\left(3 \pm i\sqrt{3}\right) \tag{A20}$$

Hence, we conclude that $k_1 = k_2 = k_3 = 0$ is not possible for real α parameter as well.